Chapter 5

Synthetic incorporation of palladium-nickel bimetallic nanoparticles within mesoporous silica/silica nanoparticles as efficient and cheaper catalyst for both cationic and anionic dyes degradation

5.1. Introduction

Recently, many research efforts have been put forth, for the development of active catalysts for the selective decomposition of toxic organic dyes via noble metal (Pt, Rh, Pd, Ru) and metal (Mo, Ni) sulphides/phosphides based nanocatalysts (Li et al., 2017; Umamaheswari et al., 2018; Al-Thabaiti, et al., 2016; Salem et al., 2018; Li et al., 2016). Since noble metals are expensive, hence efforts have been directed for making efficient noble metal nanoparticles and transition metal alloy/multimetallic analogues for most of the broad applications. To address cost-related issues, transition metals of 3d series, such as Ni, were explored for their catalytic activity to produce more economically viable and multipurpose catalysts (Qiao et al., 2012). Nickel nanoparticles have been prepared using various synthetic pathways and were studied for catalytic reactions. However, Ni nanoparticles have few major drawbacks. They undergo rapid oxidation to their oxides, rendering the surface of nanoparticles inactive (Oliaee et al., 2016). Additionally, Ni^{2+} has an extremely low electrode reduction potential, so it requires a strong reducing agent for its conversion to Ni^0, viz $NaBH_4$, etc. It is well known that strong reducing agents trigger the rapid formation of nuclei, favouring the formation of aggregates, which offers instability and poor dispersibility of nanomaterials. To enhance the properties of Ni nanoparticles, they were combined with noble metals (Pd/Pt) to form Ni_xPd_y bimetallic nanoparticles and showed improved catalytic behaviour (Du et al., 2015). However, inconsistent results were obtained due to long-term instability and loss of the desired efficiency. To serve the targeted requirements, we report herein the synthesis of Ni_xPd_y, following an advanced synthetic procedure involving the role of functional alkoxysilanes

behaving as potential micelles for nanoparticle stabilization and serving as a template for stabilizing and formation of Pd-Ni bimetallic nanocrystallite. We have demonstrated the role of 3-Glycidopxypropyltrimethoxysilane (3-GPTMS) and other functional alkoxysilanes like 3-aminopropyltrimethoxysilane (3-APTMS) and 3-(2-(3,4 Epoxycyclohexyl) ethyl-trimethoxy silane (EETMS) in the synthesis and stabilizing the noble metal nanoparticles collected playing a key role in the conversion of noble metal cations to zero-valent species in the presence of various organic reducing agents (Pandey et al., 2014b and c; Pandey et al., 2015b; Pandey et al., 2016c). The functional trialkoxysilanes likely to undergo self assemble over mesoporous silica particles/mesoporous silica nanoparticles, thus serving as a template for stabilizing the nanocrystallite within the mesoporous support. Accordingly, we have made the monometallic Pd, and their bimetallic Ni_xPd_y analogues with Ni and Pd in different molar ratios (1:1, 5:1) within mesoporous support via functional alkoxysilanes mediated synthetic incorporation of palladium nanoparticles within mesopores, serving as an active platform for stabilizing Ni-Pd nanocatalyst within the mesoporous system. The requirement for enhancing the practical usability and faster catalytic applications again directed us to use mesoporous silica nanoparticles enabling the homogenous distribution of heterogeneous nanocatalysts within the reaction medium that may further allow to enhance and control the active surface area for real applications. Despite the fact that we previously reported the design of a Pd-nanoparticles-encapsulated silica-alginate bead (Pandey et al., 2017). However, the incorporation of Ni, along with Pd, has not been found compatible for such incorporation within such support. Accordingly, an attempt has been made to explore other efficient porous matrices that may efficiently allow the assembling of Ni-Pd nanocatalyst for practical application. The use of

mesoporous silica for making mesoporous silica-Cu_2O-graphene nanocomposite via the self-assembly method has been demonstrated (Nguyen et al., 2018), for cationic-anionic dye pollutants. Cu_2O-graphene oxide inserted mesoporous silica helped in the photodegradation of dye within the time span of 180 min, apart from the significant advantages of sol-gel process derived silica. The use of mesoporous silica particles (MSPs)/mesoporous silica nanoparticles (MSNPs) may be more suitable materials for the fabrication of Ni-Pd supported nanocatalyst when alkoxysilanes are explored as a potential reducing agent for the reduction of palladium cations since silanol group derived from such moiety may undergo assembling with porous silica along with stabilization of mono and bimetallic nanoparticles within mesoporous system yielding into an efficient catalytic product for better practical applications. The use of MSPs/MSNPs for assembling the Ni-Pd nanocatalyst seems to be more reasonable from following angles; (i) mesoporous matrix may facilitate the assembling of Ni-Pd nanocatalyst, (ii) The use of functional alkoxysilanes during nanoparticles synthesis may allow selective interaction through sol-gel processing yielding Silica-MSPs/MSNPs formulation with enhance stability of the nanocrystallite for practical application, (iii) the availability of mesoporous structure may facilitate the better incorporation of bimetallic nanocrystallite, (iv) Silica-MSPs/MSNPs matrix may further be regenerated for subsequent catalytic applications, (v) the use of silanol suspension during supported nanocatalyst fabrication may behave as binder for fabricating the mesoporous supported nanocatalyst in desired size for efficient, practical application that can be restored after many use followed by regeneration of catalytic activity through easy separation and (vi) the use of mesoporous silica nanoparticles may further enable faster degradation dynamics as compared to that for relatively larger mesoporous silica

particle. The current finding demonstrates a process for fabricating the mesoporous silica/mesoporous silica nanoparticles assembled nickel-palladium bimetallic nanocrystallite for selective catalytic application in cationic-anionic dye degradation. Industries like textiles, leather, and food discharge huge quantities of toxic pollutants into the natural water source and this wastewater creates major environmental problems as many dyes are toxic, human carcinogen, mutagenic due to the very complex structure of dyes (Banazadeh et al., 2016; Singh et al., 2016; Beshkar et al., 2017). Notably, a different type of synthetic dye inclosing chromophore structures causes severe problems for both flora and fauna (Ameen et al., 2016; Matouq et al., 2014). In general, both cationic and anionic dyes are reported to be potent environmental pollutants, directly affecting the physiological processes of humankind (Wang et al., 2011). even at low quantity. Consequently, the complete removal of these non-biodegradable organic dyes from wastewater has been one of the substantial environmental issues and directed to explore efficient catalysts that may allow the rapid degradation of these pollutants in real-time. Recently, many methods have been used to remove hazardous dyes, including ion exchange coagulation-flocculation, adsorption, and biological methods, these techniques are more costly due to the complex structure of dyes. (Xu et al., 2018; Mohamed et al., 2019). However, it is required to generate a new low-cost method for dye degradation. New techniques could help us optimise wastewater treatments to get the highest quality of water (Samaei et al., 2018). In this study, mesoporus silica particle (MSPs) and mesoporous silica nanoparticles (MSNPs) are made providing an excellent platform for incorporating nickel-palladium bimetallic nanocrystallite for rapid real-time degradation of such toxic dyes. The mesoporous silica support of two different particle sizes, i.e., 50 mm and 200 nm, with pore

size 6 nm and 4 nm respectively are chosen for such a degradation study that yielded the real-time degradation of both cationic and anionic dyes within less than 3 min. The finding on the synthetic incorporation of nickel-palladium bimetallic nanocrystallite within mesoporous support has been identified by TEM, EDX, XRD, and elemental mapping. Congo red as an anionic dye and rhodamine as a cationic dye are explored for degradation study. Pore diameter, pore-volume, and surface area of nickel-palladium bimetallic nanocrystallite supported MSPs were determined via nitrogen adsorption/desorption isotherms using the BET method. A comparative kinetic study justifying the significance of MSPs and MSNPs is presented justifying real-time degradation of toxic dyes are reported in this article. Typical results on catalytic degradation of samples collected from the textile industry in Varanasi exploring the use of these dyes in printing handloom textiles via screen printing are also reported along with typical findings based on high resolution mass spectroscopy (HR-MS). The fluorescence activity of both Rh B and Congo red is well documented (Li et al., 2017; Tang et al., 2018; Bommel et al., 2007), and it directed us to examine the fluorescence of the same before and after the degradation to understand the nature of by-product formation during catalytic degradation. Interestingly, the results yielded excellent findings and were reported in this article based on 2D and 3-D fluorescence imaging that justified the formation of a highly fluorescent biphenyl by-product during the degradation of Congo red, whereas a non-fluorescent product was formed during Rh B degradation. The results on these lines are reported herein.

5.2. Experimental section

5.2.1. Materials and reagent

3-Aminopropyletrimethoxy silane (APTMS), tetrachloropalladate (K_2PdCl_4), formaldehyde, sodium borohydride ($NaBH_4$), ethylene glycol, and methanol were obtained from Sigma Aldrich. Nickel sulphate hexahydrate ($NiSO_4.6\ H_2O$) was obtained from Himedia and all the experiments were performed using double distilled water. Mesoporous silica pore size 6 nm and the average particle size 50 μm was obtained from Fluka.

5.2.2. Synthetic incorporation of palladium nanoparticles within mesoporous silica (MSPs) and mesoporous silica nanoparticles (MSNPs)

Synthesis of PdNPs inserted MSNPs/MSPs described in **chapter 4** in a **section 4.2.5.**

5.2.3. Synthesis of Pd-Ni bimetallic nanoparticles inserted MSNPs/MSPs

Synthesis of Pd-Ni NPs-1 and Pd-Ni NPs-2 inserted MSNPs/MSPs described in **chapter 4** in a **section 4.2.6.**

5.2.4. Instrumentation

The as-synthesized bimetallic nanocrystallite inserted MSNPs/MSPs and also monometallic nanoparticles were characterized by HR TEM (Hitachi 800 and 8100) with an acceleration voltage of 200 kV. The sample was diluted with double distilled water and ultra-sonicated for 15 min before placing over the carbon-coated grid for sample characterization. The elemental confirmation was characterized by FE SEM analysis (Nava nano SEM 450), EDX, and elemental mapping. The degradation of dyes was monitored by using a UV-Vis-spectrophotometer (Hitachi U-2900). 2 D and 3D Fluorescence of Congo red and Rh B were

measured using Hitachi F7000. AB Sciex 4800 plus MALDI TOF-TOF Analyzer was used for identification of Rh B and Congo red undegraded and degraded product. Similarly, the surface area analysis, pore-volume, and average pore diameter were done by the Brunauer-Emmet-Teller (BET) method using Bellsorp Max II ads-des at 77k instruments. The Rigaku X-ray diffractometers (SMARTLAB, RIKAGU Corporation, Japan) instrument was used to measure the XRD pattern of the synthesized sample.

5.2.5. Measurement of cationic and anionic dyes degradation

Both anionic dyes as Congo red and cationic dye Rhodamine (Rh B) were used for catalytic degradation using PdNPs, Pd-Ni NPs-1, and Pd-Ni NPs-2 nanocrystallite inserted MSNPs and MSPs.

5.2.5.1. Pd-Ni inserted MSNPs mediated degradation of Congo red

55 ppm aqueous solution of Congo red was added into standard quartz cuvette (1 cm path length) followed by the addition of 3 mg Pd-Ni NPs-1 inserted MSNPs. The UV-Vis absorption spectra between 250–700 nm (Hitachi 2900) was recorded just before adding the catalyst followed by recording the same just after the addition of catalyst and subsequently at constant interval till the absorption at 496 nm is decreased to a constant plateau. A similar procedure was adopted for Congo red degradation with Pd-Ni NPs-2 inserted MSNPs and MSPs.

5.2.5.2. Pd-NI inserted MSNPs mediated degradation of Rhodamine (Rh B)

An aqueous solution of Rh B (15 ppm) was added into standard quartz cuvette (1 cm path length) followed by the addition of 3 mg Pd-Ni NPs-1 inserted MSNPs. The UV-Vis absorption

spectra between 250 – 700 nm (Hitachi 2900) were recorded just before adding the catalyst followed by recording the same just after the addition of catalyst and subsequently at constant interval till the absorption at 552 nm is decreased to a constant plateau. A similar procedure was adopted for Rh B degradation with Pd-Ni NPs-2 inserted MSNPs and MSPs. Similar experiments with only PdNPs inserted MSNPs/MSPs were carried out for both Rh B and Congo red.

6.3. Results and discussion

5.3.1. Synthesis and characterization of Pd-Ni bimetallic nanocrystallite inserted MSNPs/MSPs.

Here exploration of both cationic and anionic dyes. The use of functional alkoxysilanes over mesoporous silica support provides a template for the synthetic incorporation of nanoparticles within the mesoporous matrix via self-assembly of silanol residue. Accordingly, functional alkoxysilanes mediated formation of palladium nanoparticles were initially sought for synthetic incorporation of Pd-Ni bimetallic nanocrytallite. During synthetic insertion of PdNPs within mesoporous support, the palladium cations were allowed for through distribution within mesopores under stirring followed by collecting the palladium cations inserted mesoporous support through centrifugation. The palladium cations inserted mesoporous support is then allowed to interact with 3-APTMS under stirring, followed by the addition of either 3-GPTMS or formaldehyde acting as a potential reducing agent for 3-APTMS treated palladium cations. The incubation under microwave for less than 1 min caused the rapid formation of PdNPs

inserted mesoporous support that can be collected by centrifugation, washing with water, and drying at 80^{o}C.

The PdNPs inserted MSNPs/MSPs were suspended in PVP stabilized aqueous solution of nickel sulphate in order to make Pd-Ni NPs inserted mesoporous support, and allowing the reduction of Ni cations by sodium borohydride. The use of 3-APTMS and 3-GPTMS provided an excellent template for yielding Pd-Ni bimetallic nanocrystallite within mesoporous support. The composition of nickel could be varied as desired. We attempted to use 1:1 (Pd-Ni NPs-1) and 1:5 (Pd-Ni NPs-2) palladium/nickel ratio during synthetic insertion of these nanocrystallites within mesoporous support and indeed system responded well for yielding nanocrystallite inserted mesoporous support.

As made PdNPs and Pd-Ni NPs inserted nanocrystallites have been examined by transmission electron microscopy as shown in Fig. 5.1. Fig. 5.1(a) and (b) show the TEM images of PdNPs inserted mesoporous silica nanoparticles justifying the efficient synthetic insertion of PdNPs within mesoporous support. Fig. 5.1(c) shows the selected area electron diffraction pattern (SAED) and confirms the presence of 111, 222, 400, and 442 planes of palladium nanoparticles. The particle size distribution as shown in Fig. 5.1(d) predicts the average size of 6 nm within mesoporous silica nanoparticles. Similarly, The TEM image Pd-Ni NPs-1 inserted MSNPs made at Pd-Ni ratio of 1:1 is shown in Fig. 5.1 (e), Fig. 5.1(f) respectively at two different magnifications. SAED as shown in Fig. 5.1(g) confirms the presence of 111, 311 planes assigned to nickel whereas 220, 420 planes are assigned the presence of palladium nanocatalyst. Fig. 5.1(h) shows the average size of Pd-Ni NPs-1 nanocrystallite to the order of 8 nm. As made PdNPs inserted mesoporous support has been

further analyzed by HR SEM as shown in Fig. 5.2. shows HR SEM image and EDX shown in Fig. 5.2 (a and b) respectively, whereas are shown the elemental mapping of various constituents are shown in Fig. 5.2(c-f) and confirms the presence of palladium and silica as significant components. HR SEM images of Pd-Ni NPs-1 inserted mesoporous support made at Pd: Ni ratio to the order of 1:1 is shown in Fig. 5.3. Fig. 5.3 shows the HR SEM image (a) and EDX (b) respectively justifying the presence of both Pd and Ni at 1:1 ratio as further confirmed by elemental mapping shown in Fig. 5. 3(c-f).

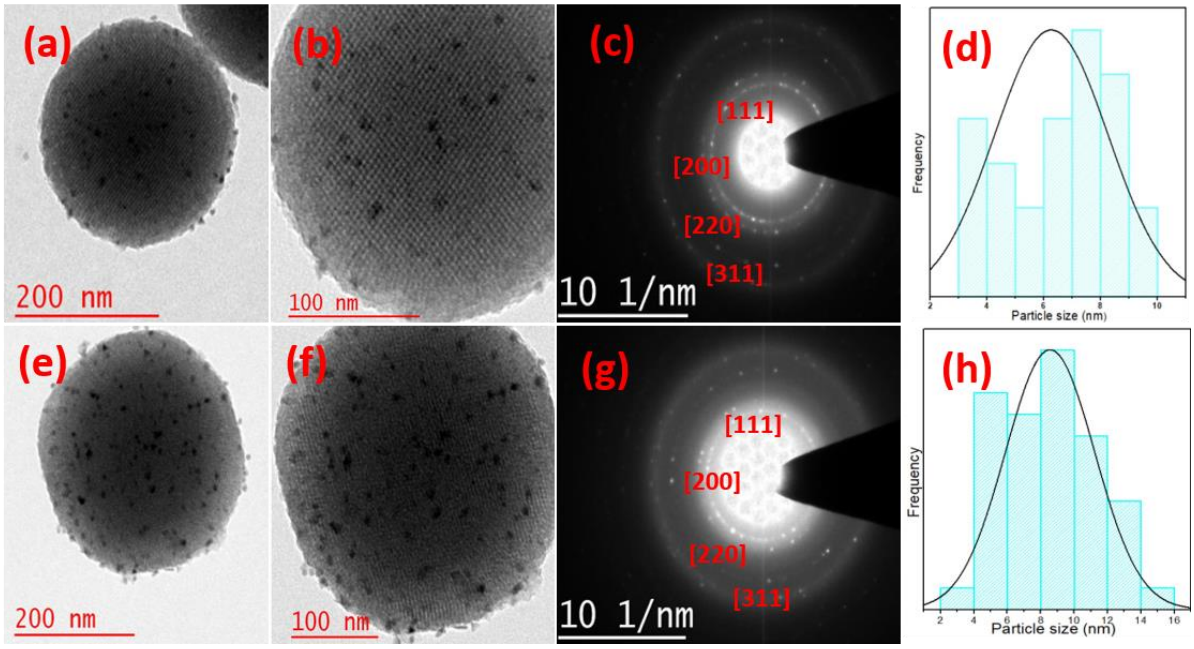

Fig. 5.1. (a), (b), TEM images of PdNPs inserted mesoporous silica nanoparticles at two different magnifications (c) Shows Selected area electron diffraction pattern and (d) represent particle size distribution curve; (e)-(f) TEM images at different magnification, (g) Shows the Selected area diffraction pattern and (h) shows the particle size distribution curve for Pd-Ni NPs-1 and inserted mesoporous silica nanoparticles.

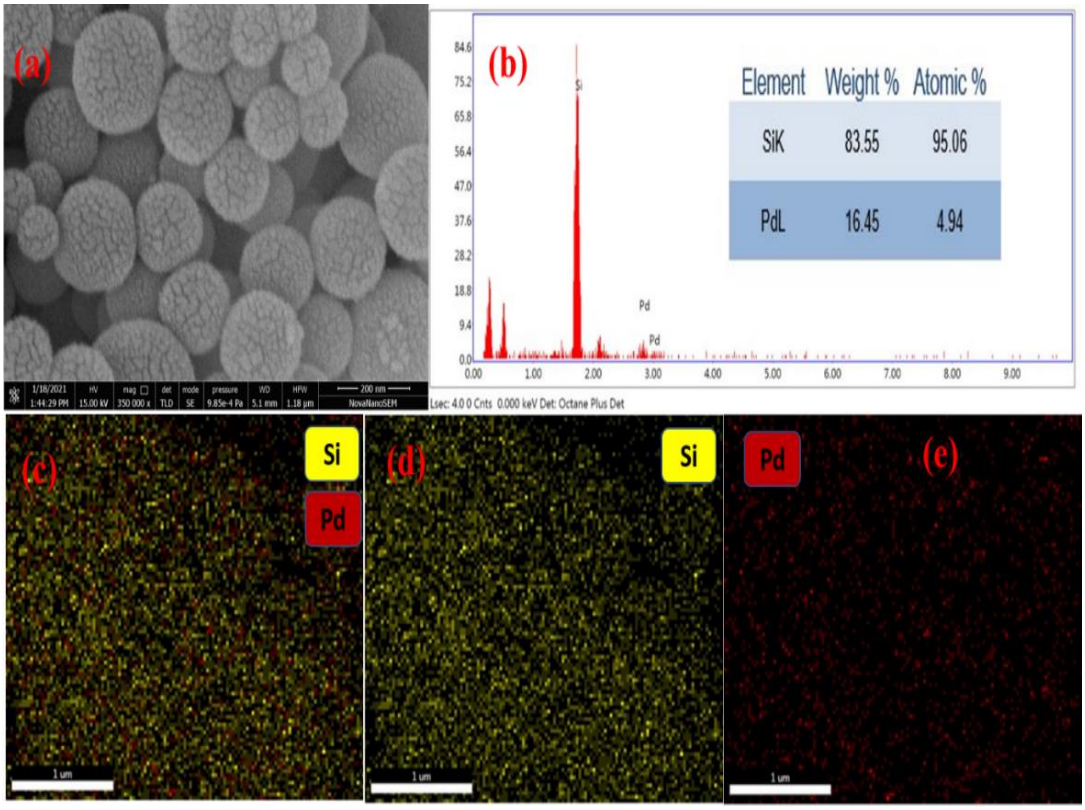

Fig. 5.2**.** (a), (b) FE SEM images and EDX of PdNPs inserted mesoporous silica nanoparticles respectively. (c)-(e) shows the elemental mapping for PdNPs nanocatalyst inserted mesoporous silica nanoparticles.

The XRD spectrum of as synthesized PdNPs nanocatalyst within MSNPs is shown in Fig. 4(a). The spectrum shows five peaks assigned to presence of (111), (200), (220), (311), and (222), set of lattice planes of Bragg reflection, which confirmed the formation of Pd-NPs nanocrystallite [JCPDS standard (88-2335)]. X-ray diffraction of bimetallic Pd-Ni NPs-1 nanocatalyst is similar to PdNPs with additional strong peak corresponding of 51.4^0 corresponding to the plane (200) of Ni which is shown in Fig.4(b) (JCPDS standard (89-7128). The XRD observation as shown in Fig.5.4 revealed the presence of two or more than two sets

of individual diffraction pattern revealing the existence of mixture or heterogeneous Pd, or Ni nanoparticles. Since stability of individual nickel nanoparticles remained in question and recorded stability discussed vide infra under section 5.3.5 predict the stabilization of Ni-nanoparticles either through the formation of Pd-Ni bimetallic within mesoporous matrix or specific interaction with silica and require further detailed investigation based on HRTEM imaging along with controlling the ratio of monomeric constituent in bimetallic configurations followed by determining their lattice constant which constitutes future projection of current thesis work .

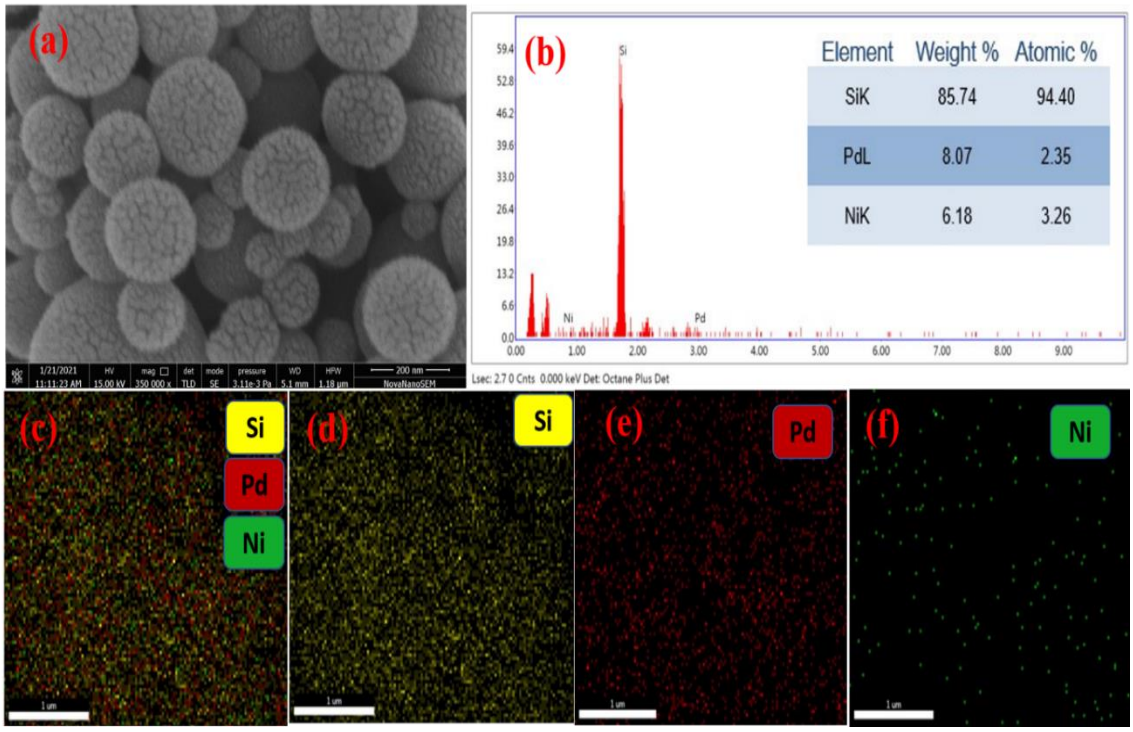

Fig. 5.3. (a), (b) FE SEM images and EDX of Pd-Ni NPs-1 inserted mesoporous silica nanoparticles respectively. (c)-(e) shows the elemental mapping for Pd-Ni NPs-1, nanocatalyst inserted mesoporous silica nanoparticles.

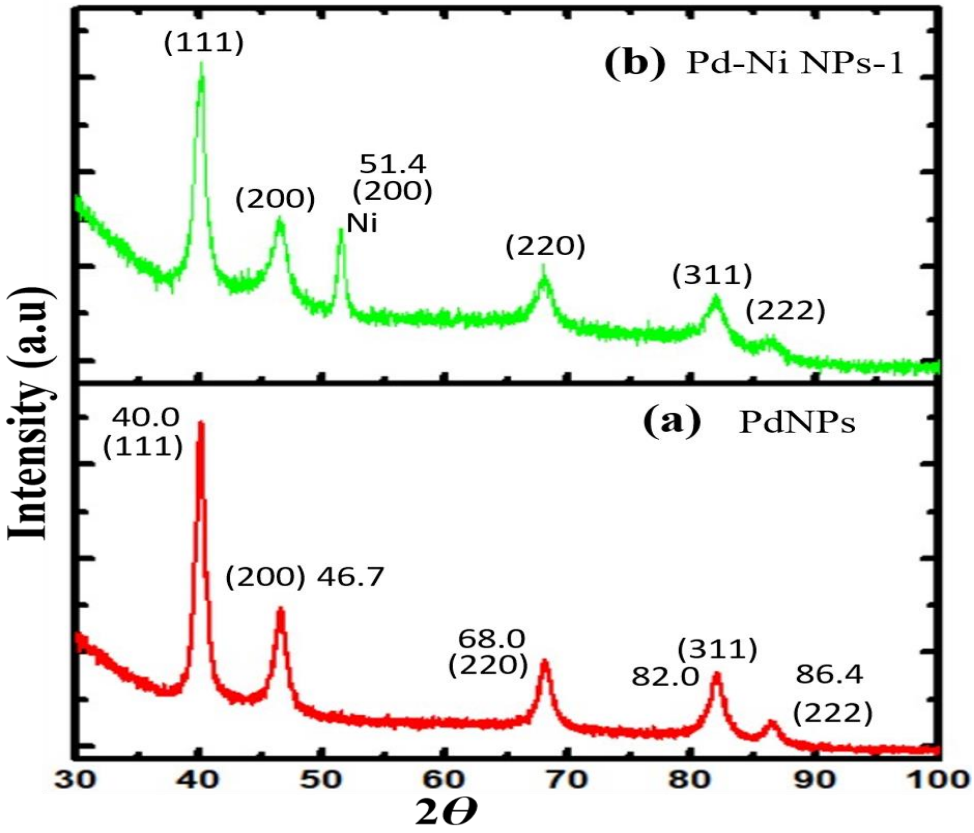

Fig. 5.4. XRD profile of (i) PdNPs inserted mesoporous silica nanoparticles (ii) Pd-Ni NPs-1 inserted mesoporous silica nanoparticles.

5.3.2. Catalytic degradation of both cationic and anionic dyes

To justify the potential application of nanocatalyst supported mesoporous matrix, both cationic and anionic dyes are explored for degradation study. Cationic Xanthene dye like Rhodamine (Rh B) and Congo red as an anionic dye are chosen for such investigation since

these dyes, even at a low level, are reported to be neurotoxic, mutagenic, carcinogenic, and irritates skin, eyes, and the respiratory tract. We have recently demonstrated that Rh B can be degraded within 1.5 min through Prussian blue nanoparticles mediated photo Fenton reaction into a colorless product based on the decrease in absorbance at 552 nm (Singh et al., 2020). Three nanocrystallites namely PdNPs, Pd-Ni NPs-1, and Pd-Ni NPs-2 inserted within MSPs are used to understand the relative catalytic efficiency for Rh B degradation based on the measurement of absorbance recorded at 552 nm as shown in Fig. 5.5. Fig. 5.5(a), (b and (c) show the results on Rh B degradation with PdNPs, Pd-Ni NPs-1 and Pd-Ni NPs-2 nanocrystallite inserted MSPs respectively. The time taken during complete degradation of Rh B is found to be 132 s, 110 s, and 144 s for PdNPs, Pd-Ni NPs-1, and Pd-Ni NPs-2 inserted MSPs respectively. Analogous observation for Congo red degradation has been recorded as shown in Fig. 5.6. Fig. 5.6(a), (b and (c) show the results on Congo red degradation with PdNPs, Pd-Ni NPs-1 and Pd-Ni NPs-2 nanocrystallite inserted MSPs respectively. The time course for Pd-Ni NPs-1 mediated degradation of 55 ppm Congo red is the order of 330 s. Justifying better catalytic activity of Pd-Ni NPs-1 inserted MSPs in dye degradation among three nanocatalyst. Accordingly, Pd-Ni NPs-1 nanocrystallite inserted MSPs were used for the degradation of both Rh B and Congo red in detail.

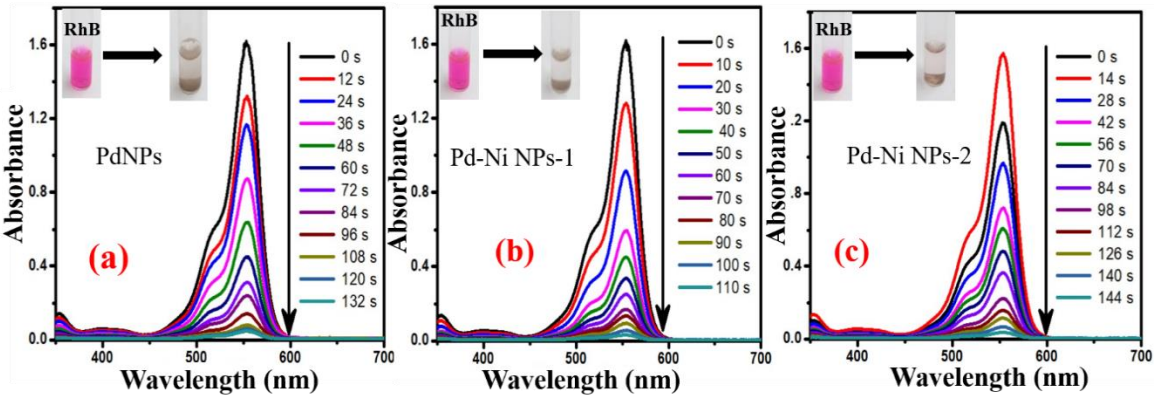

Fig. 5.5. UV-vis absorption spectra of **(a)** PdNPs **(b**) Pd-Ni NPs-1 **(c)** Pd-Ni NPs-2 inserted mesoporous silica particle (MSPs) of diameter 50 μm mediated degradation of 15 ppm Rh B.

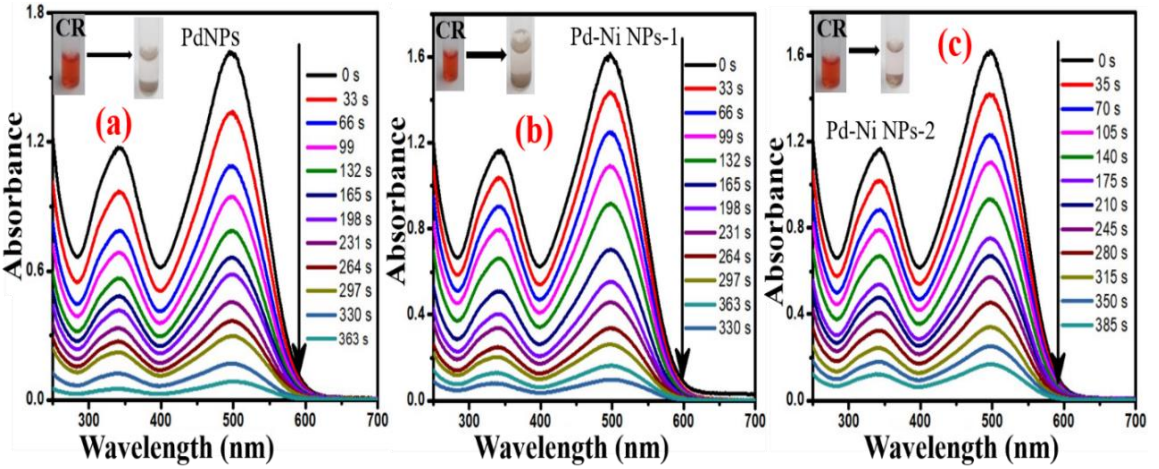

Fig. 5.6**.** UV-vis absorption spectra of (a), PdNPs (b), Pd-Ni NPs-1 **(**c) Pd-Ni NPs-2 inserted mesoporous silica particle (MSPs) of diameter 50 μm mediated degradation of 55 ppm Congo red.

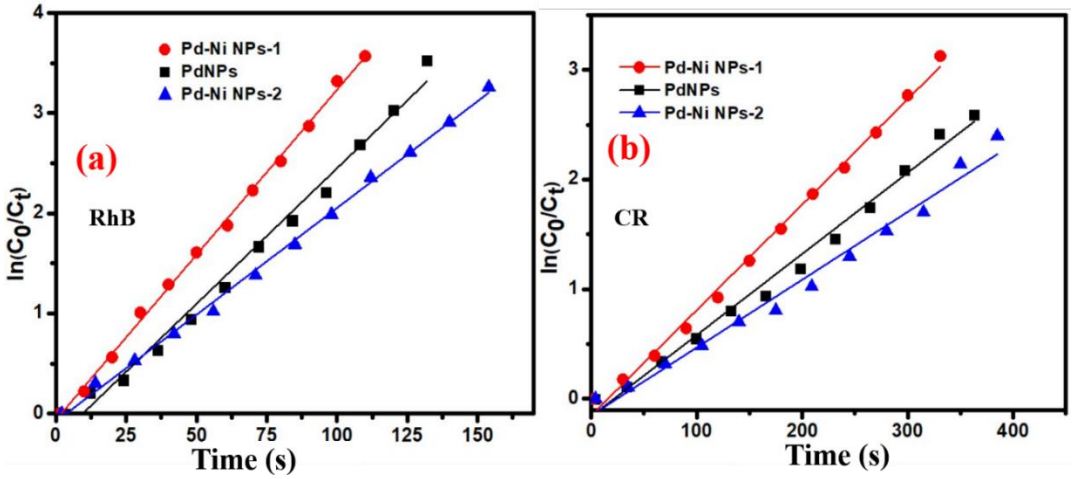

Fig. 5.7. Plot between the $\ln(C_0/C_t)$ Vs time curve and linear fitting for (a) Rh B and (b) Congo red show for PdNPs, Pd-Ni NPs-1, and Pd-Ni NPs-2 inserted mesoporous particles supported nanocatalysts.

The results as shown in Fig. 5.7(a) and Fig. 5.7(b) are explored for evaluating the rate constants for catalytic degradation of PdNPs, Pd-Ni NPs-1 and Pd-Ni NPs-2 inserted mesoporous support. The plot between $\ln(C_0/C_t)$ Vs time curve based on a linear fit for Rh B and Congo red is shown in Fig. 5.7(a) and (b) respectively for PdNPs, Pd-Ni NPs-1, and Pd-Ni NPs-2 inserted mesoporous supported nanocatalyst. The catalytic efficiency is found to the order of Pd-Ni NPs-1 >PdNPs>Pd-Ni NPs-2 supported MSPs. The data on apparent rate constant is given in table-1 justifying better catalytic activity of Pd-Ni NPs-1 supported mesoporous matrix made with mesoporous silica particles of 50 μm particle diameter. It is now important to understand the role of mesoporous silica nanoparticles as support for catalytic degradation of these toxic dyes.

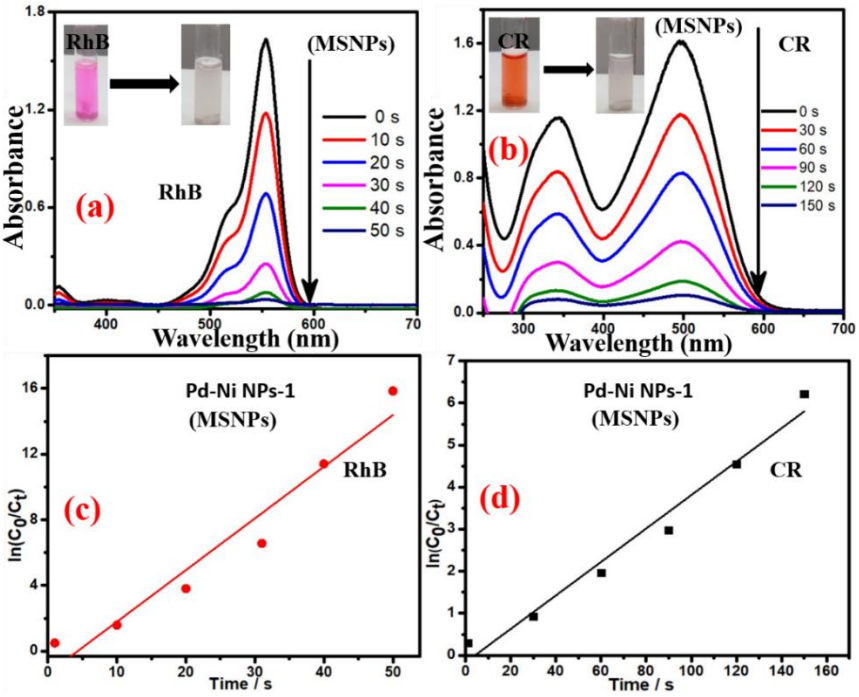

Fig. 5.8. UV-vis absorption spectra of Pd-Ni NPs-1 inserted mesoporous silica nanoparticles (MSNPs) diameter 200 nm mediated degradation of (a) Rh B and (b) Congo red. Plot between the $\ln(C_0/C_t)$ Vs time curve and linear fitting for (c) Rh-B and (d) Congo red, show for Pd-Ni NPs-1, inserted mesoporous silica nanoparticles (MSNPs) diameter 200 nm supported nanocatalysts.

Accordingly, we used mesoporous silica nanoparticles of average particle size to the order of 200 nm for the synthetic insertion of Pd-Ni NPs-1 nanocrystallite. Fig. 5.8(a) shows the results on Pd-Ni NPs-1 inserted MSNPs for catalytic degradation of Rh B, whereas Fig. 5.8 (b**),** show a similar finding for Congo red degradation. The time course required for complete degradation of these dyes under similar experimental conditions was significantly reduced to the order of 50 s for Rh B and 150 s for Congo red respectively. The plot between $\ln(C_0/C_t)$ Vs time curve based on a linear fit for Rh B and Congo red is shown in Fig. 5.8(c) and (d) respectively for

Pd-Ni NPs-1 and inserted MSNPs. The data on apparent rate constant for Pd-Ni NPs-1 inserted MSNPs are given in table-1 justifying better catalytic activity of Pd-Ni NPs-1 supported MSNPs.

Nanocatalyst	**Apparent rate constant (s^{-1})**			
	Nanocatalyst inserted Mesoporous silica Particles (50μm) for the degradation of		**Nanocatalyst inserted Mesoporous silica Nanoparticles (200 nm) for the degradation of**	
	Congo red (CR.)	Rhodamine (Rh B)	Congo red (C R)	Rhodamine (Rh B)
PdNPs	$7.4 \pm 0.35 \times 10^{-3}$	$2.6 \pm 0.31 \times 10^{-2}$	$1.4 \pm 0.28 \times 10^{-2}$	$5.1 \pm 0.25 \times 10^{-2}$
Pd-Ni NPs-1	**$9.6 \pm 0.19 \times 10^{-3}$**	**$3.2 \pm 0.14 \times 10^{-2}$**	**$1.9 \pm 0.2 \times 10^{-2}$**	**$6.9 \pm 0.21 \times 10^{-2}$**
Pd-Ni NPs-2	$6.1 \pm 0.25 \times 10^{-3}$	$2.2 \pm 0.30 \times 10^{-2}$	$1.3 \pm 0.12 \times 10^{-2}$	$4.3 \pm 0.18 \times 10^{-2}$

Table 5.1. Summary of the apparent rate constants for the reduction of CR and Rh B in the presence of nanocatalyst inserted mesoporous silica and mesoporous silica nanoparticles.

The next stage of the current investigation is to understand the effectiveness of catalytic degradation of these nanocatalyst embedded mesoporous support based on BET analysis. The nitrogen adsorption-desorption isotherms of PdNPs and Pd Ni NPs-1 inserted mesoporous silica of particle size 50 μm is depicted in Fig. 5.9 (a). These nanocatalyst exhibits type IV isotherm with Hysteresis loop of type H1, resulting from the capillary condensation of nitrogen in the mesopores, which was indicated the condensation of nitrogen within the mesopores of mesoporous silica. The isotherms of PdNPs inserted mesoporous silica, and Pd-

Ni NPs-1 inserted mesoporous silica displayed at a relative pressure of 0.45-0.83 indicating the presence of mesopores in the nanocatalyst. Pore size distribution resolved from Brunauer-Joyner-Halenda (BJH) theory is located in the range of 2 nm to 20 nm, but the foremost pore size distribution peak is marked at 10 nm for both PdNPs and Pd-Ni NPs-1 which is shown in Fig. 5.9 (b) The homogeneous distribution of nanocatalyst inserted within silica nanoparticles within the working medium displaying much faster kinetics data as shown in table-1. The results of pore parameters and surface area for the investigated nanocatalyst inserted mesoporous silica are shown in table-5.2. The surface area of PdNPs inserted mesoporous silica is increased during the formation of Pd-Ni NPs-1, enabling faster degradation of the porous nanocatalyst as compared to that for PdNPs inserted porous support.

Nanocatalyst	Specific BET surface m^2g^{-1}	Pore volume cm^3g^{-1}	Average pore diameter (nm)
PdNPs-inserted mesoporous silica (Particle size = 50 μm)	230	0.151	4.68
Pd-Ni NPs-1 inserted mesoporous silica (Particle size = 50 μm)	718	0.342	3.49

Table 5.2**.** Pore parameter of nanocatalyst inserted mesoporous silica of size 50 μm

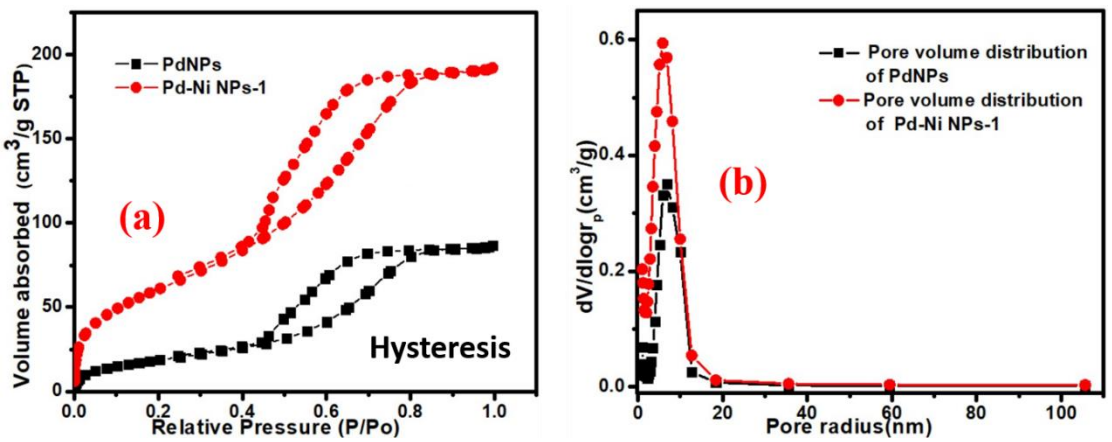

Fig. 5.9. (a) N_2 adsorption-desorption isotherms of PdNPs (i) and Pd-Ni NPs-1 (ii) inserted mesoporous silica particle; (b) Pore volume distribution curve of PdNPs and Pd-Ni NPs-1 inserted mesoporous silica particle.

5.3.3. Mechanism of nanocatalyst supported mesoporous silica mediated dye degradation

The next stage of the current investigation is to understand the process of mesoporous supported nanocatalyst for dye degradation. Since both dyes are fluorescent accordingly, nanocatalyst inserted mesoporous silica nanoparticles could be explored to understand the formation of the by-product of dye degradation. Fig. 5.10(a) shows the fluorescence spectra of Rh B before (i) and after degradation (ii). The finding, as shown in Fig. 5.10(a), predicts that the by-product of Rh B degradation is not fluorescent. 3-D fluorescence imaging of Rh B before (Fig. 5.10(d) and after degradation (Fig. 5.10(e) also revealed the formation of a non-fluorescent product during mesoporous catalyst mediated degradation justifying the mechanism as proposed in scheme-1. However, the fluorescence spectra of Congo red before and after degradation as shown in Fig. 5.10(b) display the formation of fluorescent by-product.

Fig. 5.10(b) shows the fluorescence of Congo red before (i) and after (ii) degradation. The finding justifies the formation of a highly fluorescent by-product. The fluorescence of degraded products is similar to that of biphenyl, as shown in Fig. 5.10(c). 3-D fluorescence imaging before and after degraded product along with biphenyl is shown in Fig. 5.10(f) and Fig. 5.10(g) respectively justifying the mechanism depicted in scheme-2.

It is also desirable to comment on the degradation product of chosen dyes during porous nanocatalyst mediated transformation of toxic dyes. Congo red and Rh B dyes are known water-soluble, and their color is red and pink respectively. This dye was chosen in this study because of its many applications for colorant in industry. Congo red and Rh B absorption peaks appear at 496 and 552 respectively. In the presence of a nanocatalyst, the peak tends to successively decrease and it becomes colorless converting absorption maxima to a flat plateau. In the case of Congo red absorbance peak exhibits due to n-π^* transition of —N=N— bond. The break-down of —N=N— bond of Congo red leads to the formation of biphenyl and aromatic amine. Similarly, Rh B transformation into leuco-rhodamine prevails during catalytic degradation. These findings support the following mechanism involved during nanocatalyst supported mesopores during Rh B and Congo red degradation.

5.3.4. Degraded end product analysized by high resolution mass spectroscopy of both cationic and anionic dyes

The results based on high resolution mass spectroscopy has been investigated to confirm the bimetallic nanocatalyst mediated dye degradation.

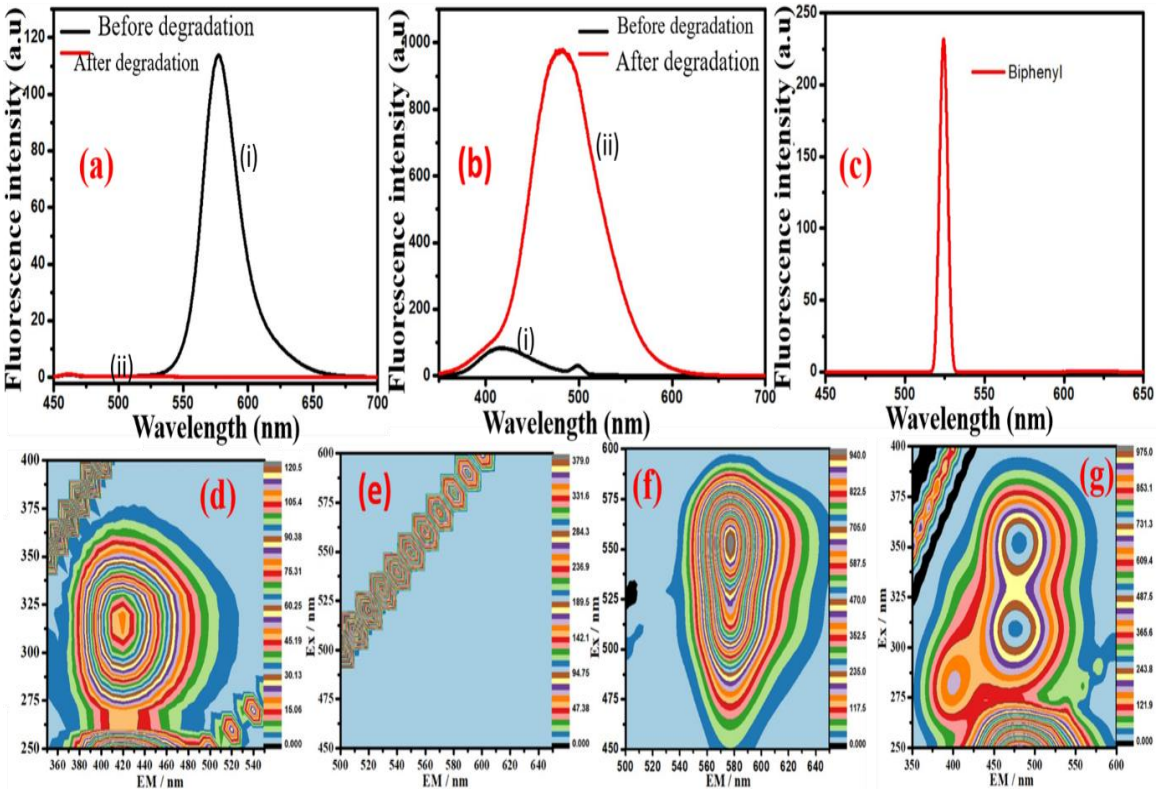

Fig. 5.10. Fluorescence spectra in absence (i) and the presence (ii) of Pd-Ni NPs-1 inserted MSNPs of (a) Rh B and (b) Congo red. Fluorescence spectra of c) biphenyl. 3-D Fluorescence spectra in absence (d) and the presence (e) of Pd-Ni NPs-1 inserted MSNPs for Rh B, 3-D Fluorescence spectra in absence (f) and the presence (g) of Pd-Ni NPs-1 inserted MSNPs for Congo red.

LC-MS analysis was used to detect and identify degraded end products. The mass spectra of both Congo red and Rh B before degradation are shown in Fig. 5.11(a) and Fig. 5.12(a) respectively whereas similar results after bimetallic nanocrystallite mediated degradation is shown in Fig. 5.11 (b) and Fig. 5.12(b) respectively.

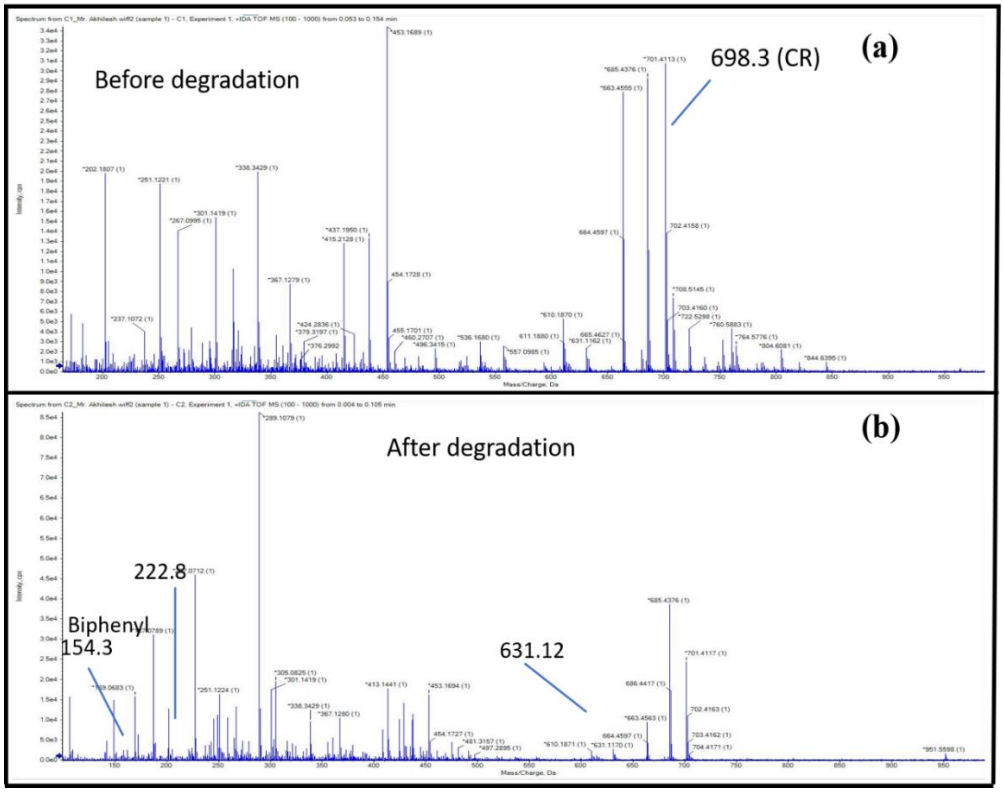

Fig. 5.11**.** HR-MS spectrum of Congo red(a) before and (b) after degradation.

For Congo red, a peak has been observed in the LC-MS spectrum with an m/z of 698. In addition to that these finding also confirm the presence of biphenyl corresponding to mass spectrogram assigned to 154 Da in Fig. 5.11(b) as observed form fluorescence spectroscopy (Fig. 5.10) out of many fragmented components of the dye. A peak for Rh B has been observed in the LC-MS spectrum at m/z 443. In addition to intermediate Rh B, the successive degraded product observed at different m/z values. Based on the mass spectrogram shown in Fig. 5.11 and Fig. 5.12, both cationic and anionic dyes were efficiently degraded using Pd-Ni supported mesoporous nanocrystallite.

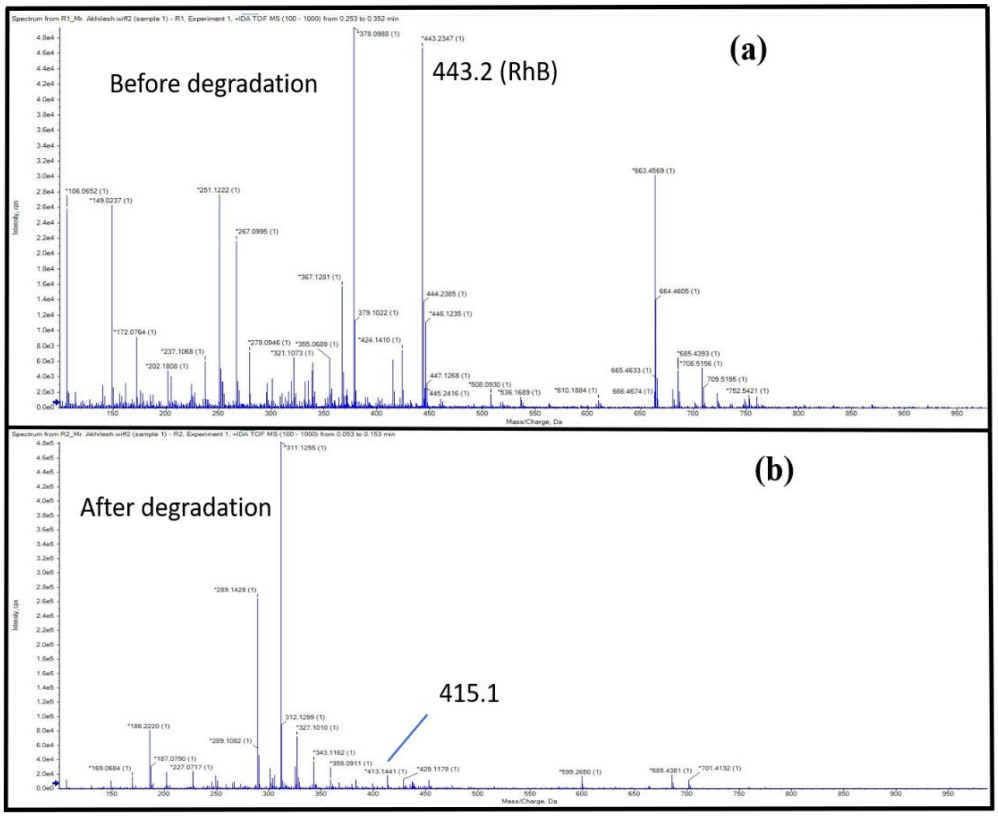

Fig. 5.12**.** HR-MS spectrum of Rh B (a) before and (b) after degradation.

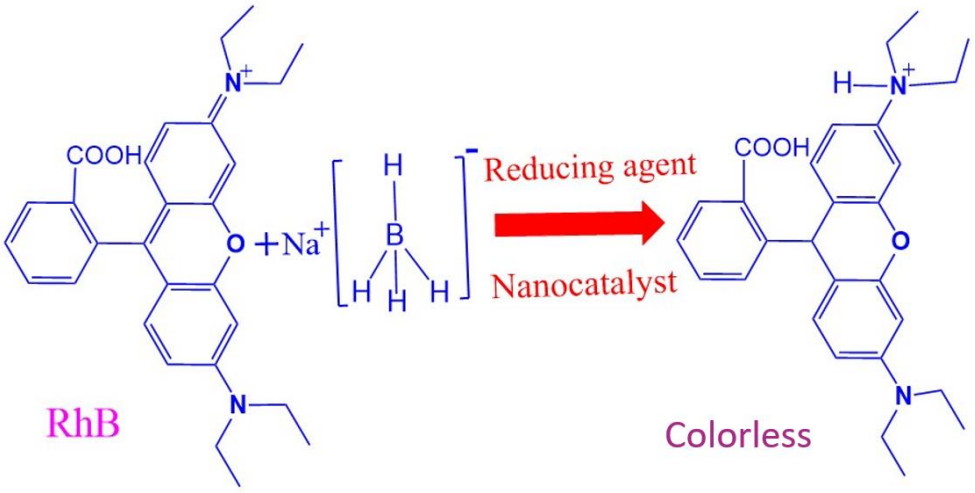

Scheme 5.1. Mechanism of Rh B degradation.

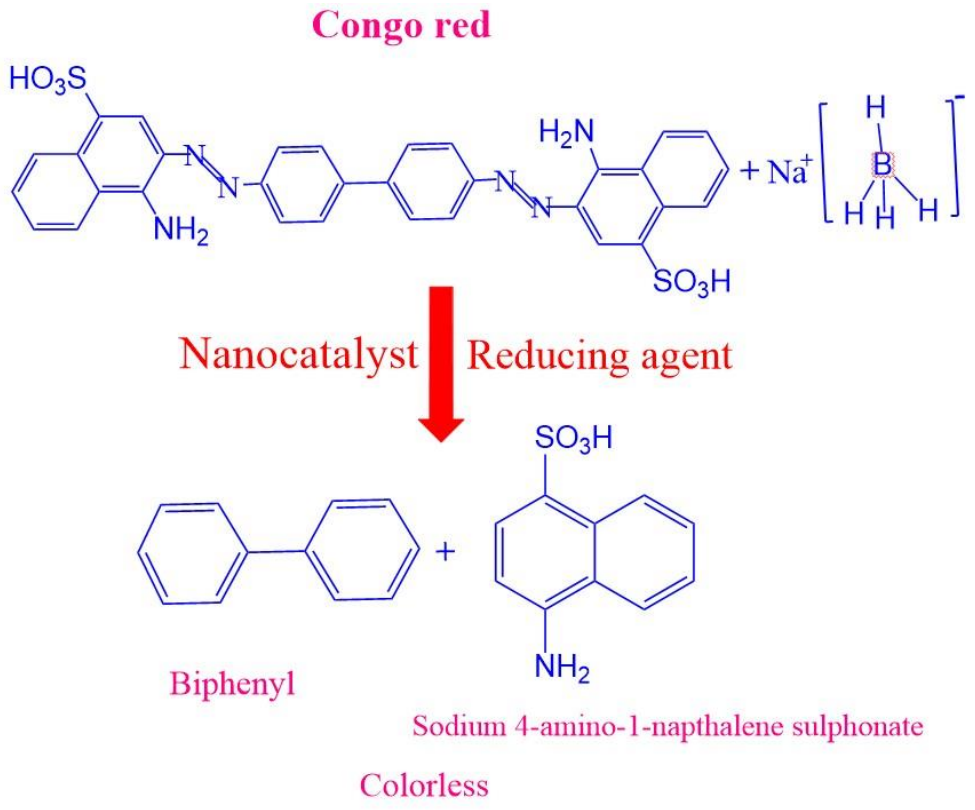

Scheme 5.2**.** Mechanism of Congo red degradation.

5.3.5. Catalyst recyclability

The nanocatalyst inserted mesoporous silica can be easily separated from the reaction system with sufficient stability and can be easily recycled with 100% catalytic efficiency by collecting the heterogeneous nanocatalyst by centrifugation followed by simple washing with ethanol and drying at 60 C^0 in a vacuum oven. This process allowed at least to recover the mesoporous nanocatalyst for 6 times for subsequent application without loss of catalytic activity.

5.3.6. Catalytic degradation of a real sample collected from the textile industry

The textile sector is the second-largest source of employment in India and consumes a huge quantity of organic dyes in manufacturing fabrics from synthetic fibers with consumption of 50-55g of dye per kg of textile products. Printed fabrics from cellulose fibers consume 85-90g per kg of textile products which are released in effluents (Yaneva et al.2012). Textile wastewater contains dyes mixed with various contaminants at a variety of ranges. Therefore, environmental legislation commonly obligates textile factories to treat these effluents before discharge into the receiving watercourses. In Varanasi, typically Handloom fabrics printed with these dyes are a common platform for these effluents. To get samples, we attempted to collect the effluent directly from the Handloom industry especially while washing the stencil with water that was used for printing these dyes embedded with a water-based binder and thinner. This original textile effluent was filtered by using the filter paper.

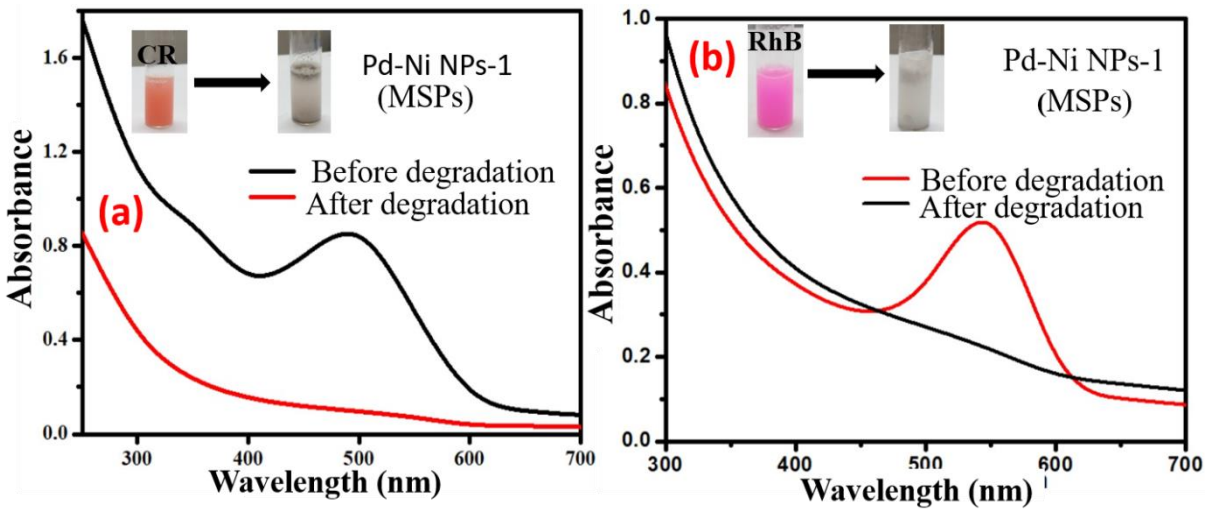

Fig. 5.13. (a), (b) shows the UV-Vis absorption spectra of the real textile sample in the absence and the presence of Pd-Ni NPs-1 inserted MSPs, for Congo red and for Rh B. The samples were collected from the washout of stencil used in fabric printing using dye embedded with binder and thinner.

5.3.7. Degradation Congo red based effluent

2 mL samples collected from the textile industry and using Congo red at dye mixed with water-soluble thinner and binder are used for catalytic degradation. The samples were filtered and 2 mL of the same was used for degradation study. The results based on UV-vis spectra, as shown in Fig. 5.13 (a), justify the complete degradation of Congo red in the presence of made Pd-Ni nanocatalyst. The typical video on catalytic degradation of a real sample can be viewed at https://youtu.be/y8bdxZNw0qE

5.3.8. Degradation Rh B based effluent

The samples containing Rh B were filtered and 2 mL of the same was used for degradation study. The results based on UV-vis spectra, as shown in Fig. 5.13 (b) justify the complete degradation of Rh B in the presence of as made Pd-Ni nanocatalyst revealing potency of porous nanocatalyst as reported earlier (Wenjun et al., 2020; Yang et al., 2019; Yang et al., 2020). The typical video on catalytic degradation of a real sample can be viewed at https://youtu.be/WQPrBKgJ1xc

5.4. Conclusions

The present article demonstrates the active role of organotrialkoxysilane in efficient reduction of palladium cations along with insitu providing a template for efficient reduction and stabilization of Pd-Ni nanocrystallite for real applications. In adiition to that use of organotrialkoxysilane further enable controlled insertion and stabilization of bimetallic Pd-Ni nanocrystallite within mesoporous silica support justifying efficient catalytic activity justifying typical application of both cationic and anioninic dyes in real time. Synthetic incorporation of these nanocatalysts within mesoporous silica particles of particle diameter 50 μm and mesoporous silica nanoparticles of 200 nm are investigated. Pd-Ni catalyst being a more efficient and cheaper catalyst and the catalytic activity of Pd-Ni bimetallic nanocatalyst made at Pd: Ni ratio of 1: 1 showed real-time degradation of both Rh B and Congo red dyes. The use of nanocatalyst inserted mesoporous silica nanoparticles yielded faster degradation to the order of 50 s for Rh B and 150 s for Congo red justifying potent catalytic behaviour for real-time degradation of toxic industrial dye. The nanocatalyst can be easily recovered retaining 100% catalytic activity for the subsequent six applications. As made catalysts allow efficient degradation of real textile effluent collected from the Handloom industry.